Supplement of Clim. Past, 17, 985–1004, 2021
https://doi.org/10.5194/cp-17-985-2021-supplement

Climate of the Past
Open Access
EGU

Supplement of

Comparison of the oxygen isotope signatures in speleothem records and iHadCM3 model simulations for the last millennium

Janica C. Bühler et al.

Correspondence to: Janica C. Bühler (jbuehler@iup.uni-heidelberg.de) and Kira Rehfeld (krehfeld@iup.uni-heidelberg.de)

List of Tables

List of Figures

Table S1. The difference between modeled and measured $\delta^{18}O$ ($\Delta\delta^{18}O = \delta^{18}O - \delta^{18}O_{dw.eq}$), corresponding to Sec. 4.1. 90% confidence intervals were calculated via bootstrapping (1000 repetitions). Maximal/minimal outliers denote those entities with the largest positive/negative difference to the simulation.

	LM1	LM2	LM3
$\Delta\delta^{18}O = \delta^{18}O - \delta^{18}O_{dw.eq}$ (global)	-0.1‰ $(-4.3, 4.2)$	-0.1‰ $(-4.3, 4.2)$	-0.1‰ $(-4.3, 4.2)$
Maximal outlier	eID598 $\Delta\delta^{18}O = 7.3$‰	eID598 $\Delta\delta^{18}O = 7.3$‰	$\Delta\delta^{18}O = 7.3$‰
Minimal outlier	eID113 $\Delta\delta^{18}O = -4.8$‰	eID113 $\Delta\delta^{18}O = -4.7$‰	eID447 $\Delta\delta^{18}O = -4.7$‰
Cluster $\Delta\delta^{18}O$			
c1 (North America)	-0.7‰ $(-5.2, 3.7)$	-0.8‰ $(-5.2, 3.7)$	-0.8‰ $(-5.2, 3.7)$
c2 (South America)	-1.8‰ $(-7.1, 3.6)$	-1.7‰ $(-7.1, 3.6)$	-1.7‰ $(-7.1, 3.6)$
c3 (Europe and Northern Africa)	0.5‰ $(-2.0, 3.0)$	0.5‰ $(-1.9, 3.0)$	0.5‰ $(-1.9, 3.0)$
c4 (Southern Africa)	-2.8‰ $(-5.44, -0.1)$	-2.8‰ $(-5.4, -0.1)$	-2.8‰ $(-5.4, -0.2)$
c5 (Arabia)	-1.3‰ $(-3.81, 1.3)$	-1.3‰ $(-3.8, 1.3)$	-1.4‰ $(-4.1, 1.3)$
c6 (India and Central Asia)	1.1‰ $(-3.6, 5.9)$	1.1‰ $(-3.63, 5.9)$	1.1‰ $(-3.6, 5.9)$
c7 (China and East Asia)	2.2‰ $(-0.2, 4.7)$	2.2‰ $(-0.2, 4.7)$	2.2‰ $(-0.2, 4.6)$
c8 (South-East Asia)	-3.0‰ $(-5.9, 0)$	-3.0‰ $(-5.9, -0.1)$	-3.0‰ $(-5.9, 0)$
c9 (New Zealand)	-1.2‰ $(-2.7, 0.3)$	-1.2‰ $(-2.7, 0.3)$	-1.2‰ $(-2.7, 0.3)$

Table S2. Improvement of median correlation c and the SNR through the selection of best age-model ensemble on different spatial levels. 90% confidence intervals through bootstrapping. For c4 Africa, no age-model ensembles were available.

Spatial aggregation level	Correlation c	Age-model tuned c_{tuned}	SNR	SNR_{tuned}
site	0.2 $(-0.0, 0.3)$	0.5 $(0.5, 0.5)$	0.3 $(-0.0, 0.4)$	1.0 $(0.9, 1.1)$
gridbox	0.22 $(0.17, 0.24)$	0.4 $(0.3, 0.5)$	0.3 $(0.2, 0.3)$	0.7 $(0.5, 1.0)$
c1 (North America)	0.1 $(-0.0, 0.2)$	0.3 $(-0.4, 0.5)$	0.2 $(0.1, 0.2)$	0.4 $(0.0, 0.9)$
c2 (South America)	-0.1 $(-0.2, -0.1)$	0.0 $(-0.4, 0.4)$	0.1 $(0.1, 0.1)$	0.0 $(0.0, 0.6)$
c3 (Europe and Northern Africa)	0.1 $(0, 0.2)$	-0.5 $(-0.6, 0.5)$	0.2 $(0.1, 0.2)$	1.1 $(0.7, 1.5)$
c4 (Southern Africa)	0.2 $(0.2, 0.2)$	NA	0.2 $(0.2, 0.2)$	NA
c5 (Arabia)	0.1 $(-0.2, 0.3)$	-0.5 $(-0.6, 0.5)$	0.1 $(0.1, 0.4)$	0.9 $(0.0, 1.1)$
c6 (India and Central Asia)	-0.1 $(-0.2, 0.2)$	-0.7 $(-0.8, 0.6)$	0.1 $(0.1, 0.3)$	2.9 $(0.1, 2.9)$
c7 (China and East Asia)	-0.2 $(-0.2, -0.1)$	-0.3 $(-0.4, 0.4)$	0.2 $(0.2, 0.2)$	0.4 $(0.0, 0.7)$
c8 (South-East Asia)	-0.2 $(-0.5, 0.3)$	-0.1 $(-0.8, 0.7)$	0.3 $(0.0, 1.1)$	0.1 $(0.1, 3.5)$
c9 (New Zealand)	0.2 $(0.2, 0.4)$	0.7 $(0.7, 1.0)$	0.3 $(0.2, 0.8)$	2.6 $(1.9, 76.1)$
global	0.1 $(-0.1, 0.1)$	0.4 $(0.3, 0.4)$	0.1 $(0.1, 0.1)$	0.5 $(0.4, 0.6)$

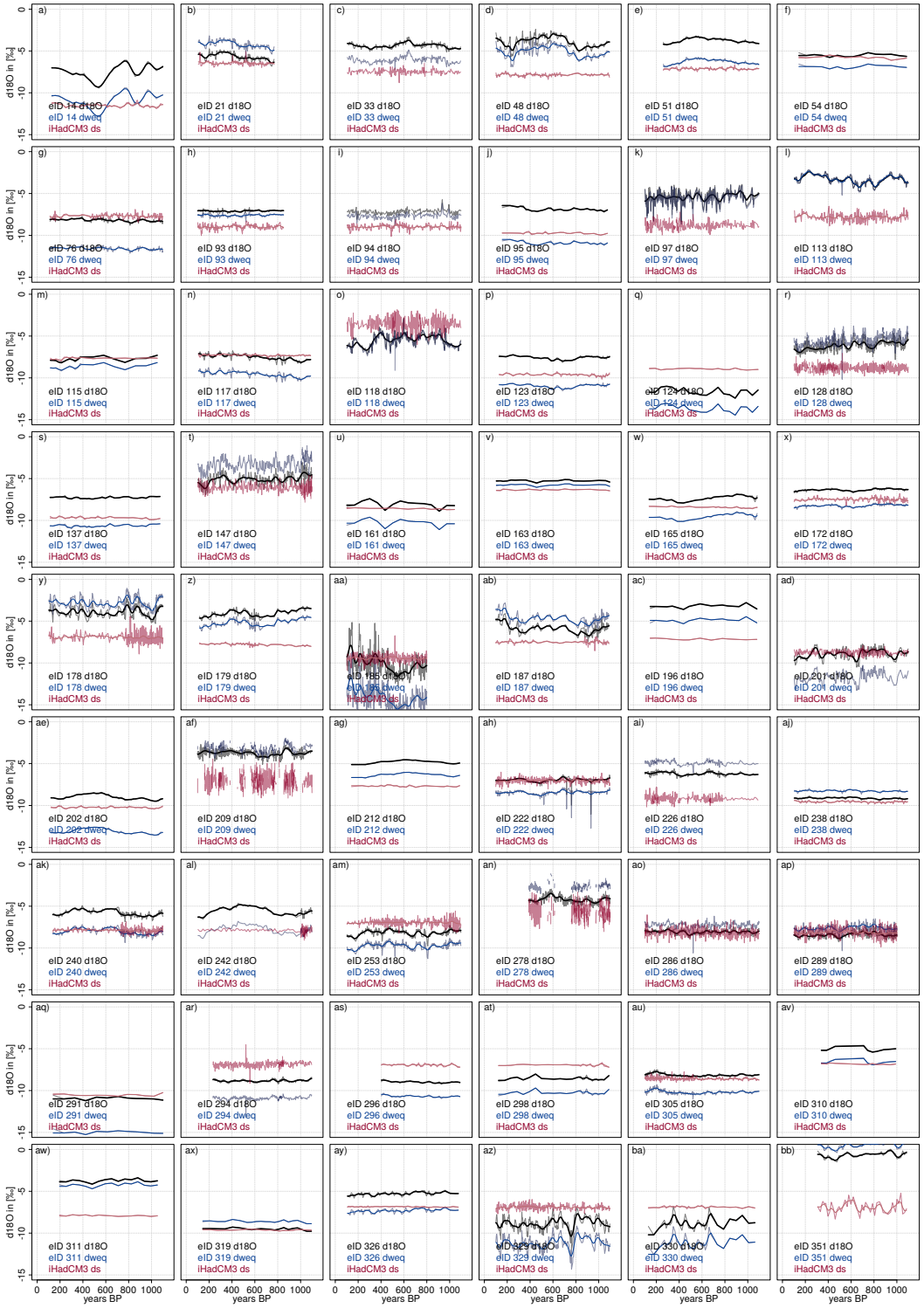

Figure S1. Time series of all analysed records for $\delta^{18}\mathrm{O}_{\mathrm{dw.eq}}$ and for simulated $\delta^{18}\mathrm{O}_{pw}$ at the cave location (Part 1, records eID 14 to eID 351).

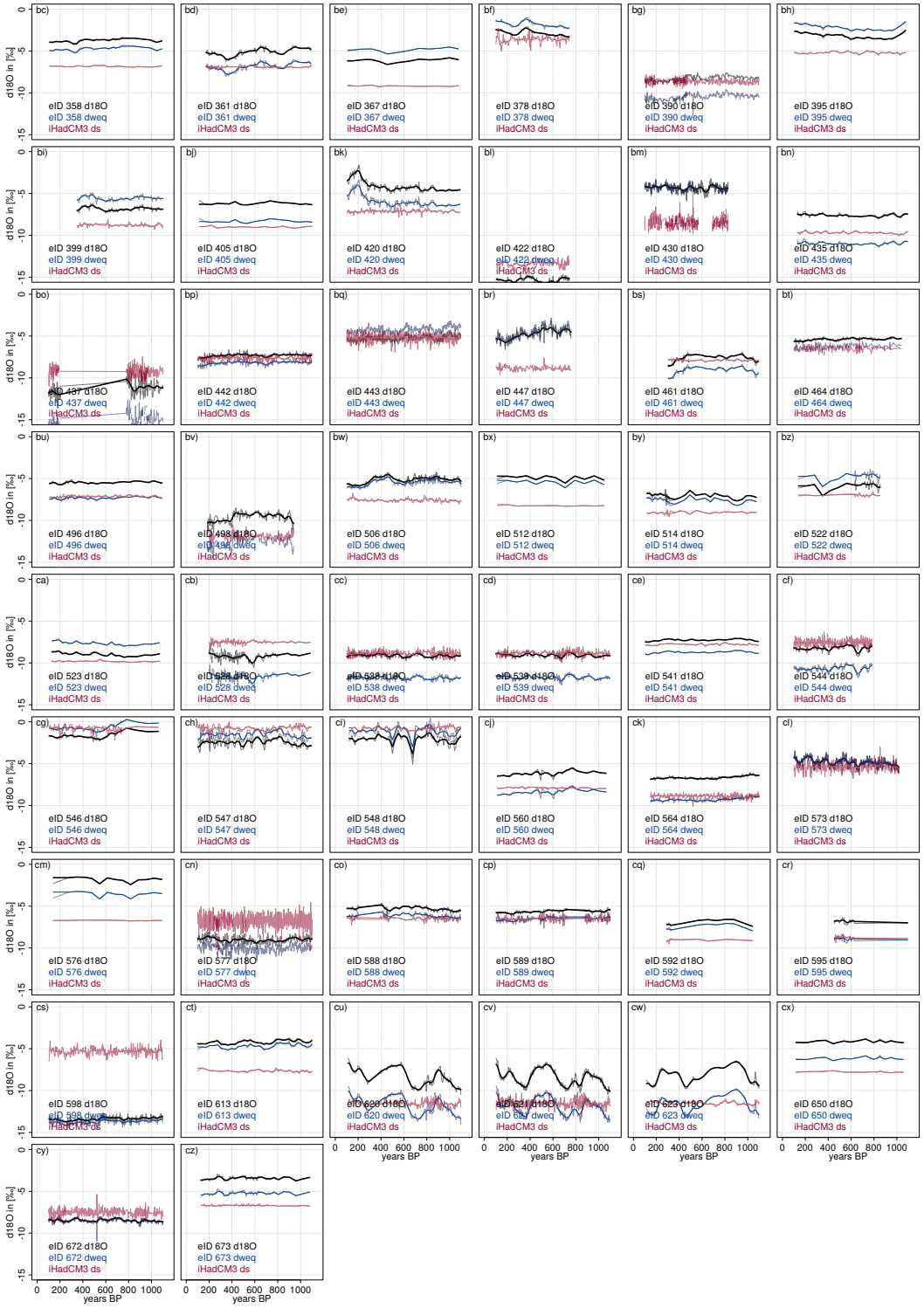

Figure S2. Time series of all analysed records for $\delta^{18}\mathrm{O}_{\mathrm{dw.eq}}$ and for simulated $\delta^{18}\mathrm{O}_{pw}$ at the cave location (Part 2, eID 358 to eID 673).

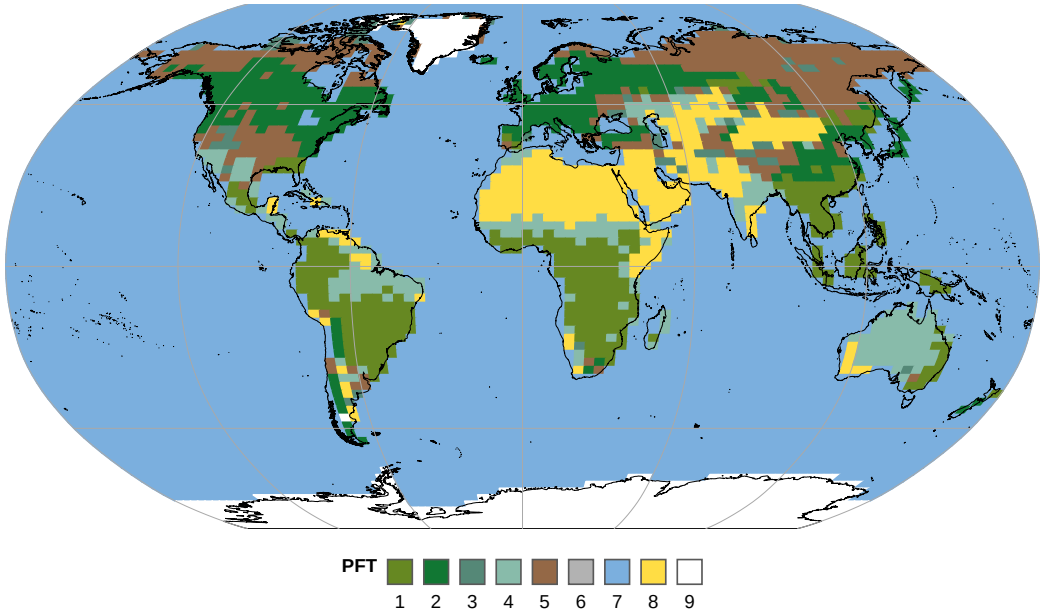

Figure S3. Dominant Plant Functional Type (PFT) of average June vegetation: The land surface and vegetation models in iHadCM3, TRIFFID and MOSES, provide nine land surface types (broadleaf trees (1), needleleaf trees (2), C3 grass (3), C4 grass (4), shrub (5), urban (6), water (7), bare soil (8) and snow/ice (9)), where each gridbox contains a fraction of each functional type. Five of these functional types are plant types. The vegetation evolves dynamically. The plot shows the dominant PFT in each gridbox.

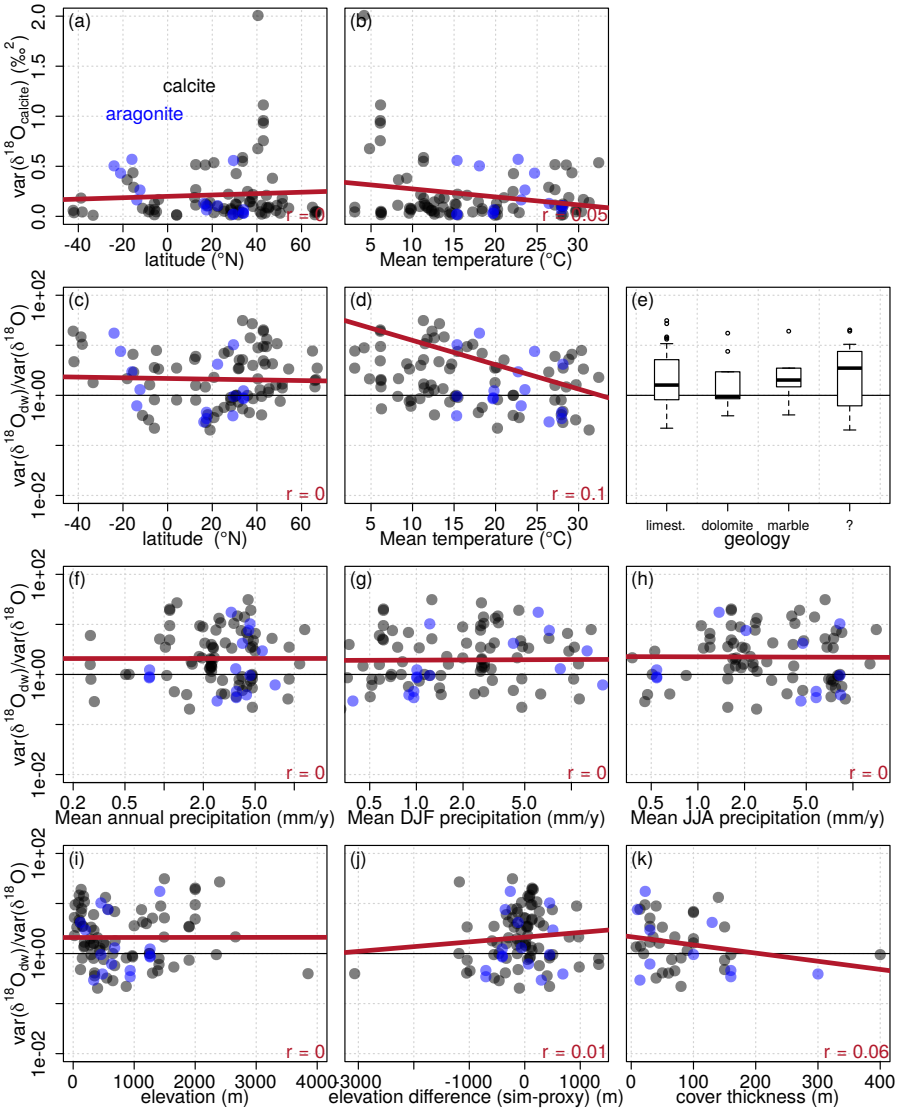

Figure S4. No relationship between variance ratio and offset: As Fig. 4 but for the ratio of recorded over simulated variance of δ^{18}O against local environmental, climatic and specimen-specific parameters.

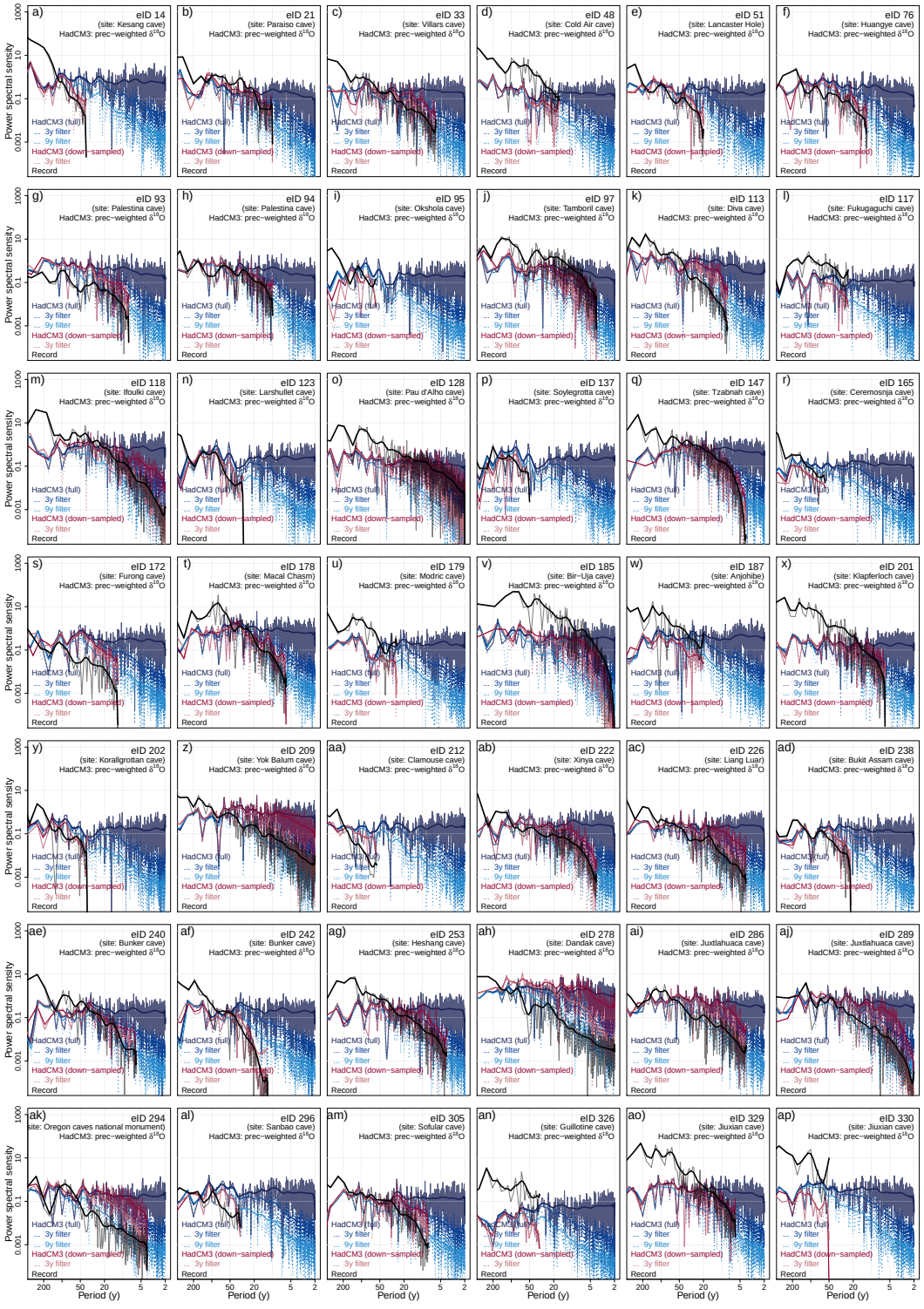

Figure S5. Spectrum for all records used in the analysis of the yearly simulation at the cave location, down-sampled to record resolution and record with the filters corresponding to Fig. 6 (Part 1, eID14 to eID390).

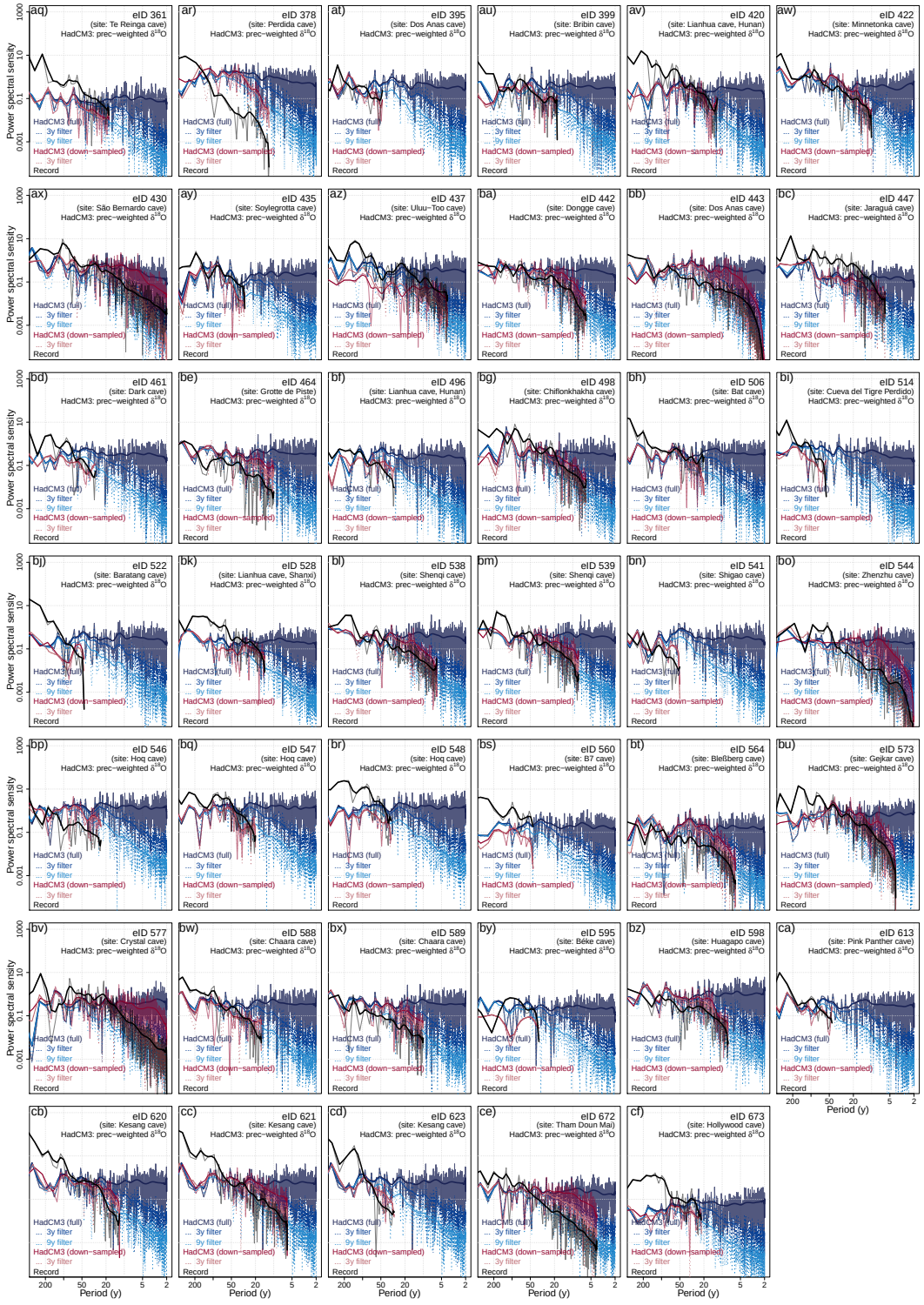

Figure S6. Spectrum for all records used in the analysis of the yearly simulation at the cave location, down-sampled to record resolution and record with the filters corresponding to Fig. 6 (Part 2, eID 399 to eID 672).

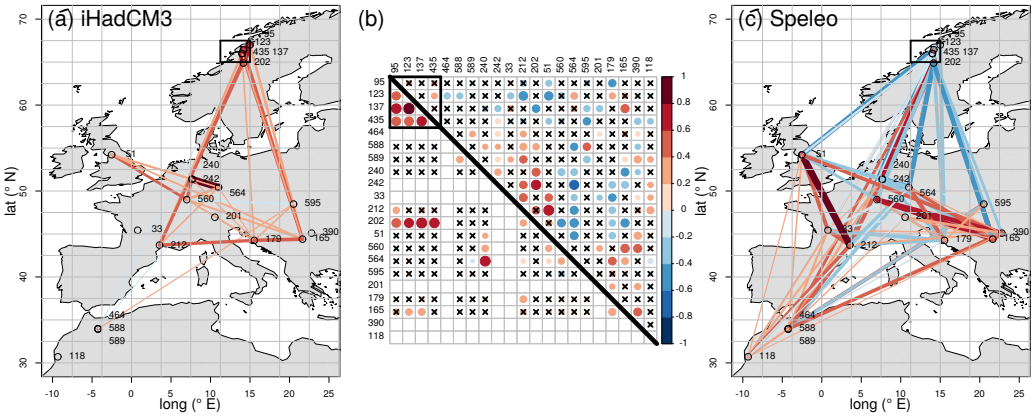

Figure S7. Network map and matrix comparison for the Europe cluster (c3) Left map (a) shows the correlation network with the simulation data which are represented as dots in the lower triangle of the correlation matrix in the middle (b). The upper triangle in (b) and the right map (c) are based on the record to record correlation. One gridbox with 4 entities is marked in the maps and the matrix to compare directly. All links with $p < 0.1$ are shown.

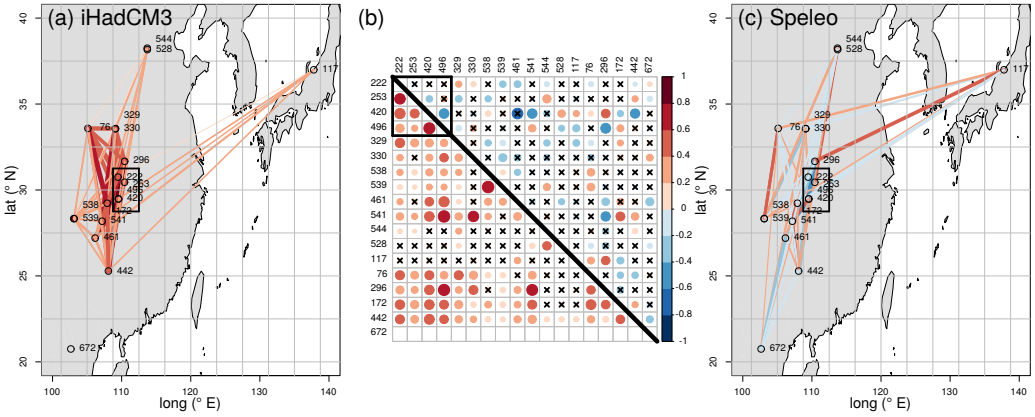

Figure S8. Network map and matrix comparison for the China and East Asia cluster (c7) as in SF7.

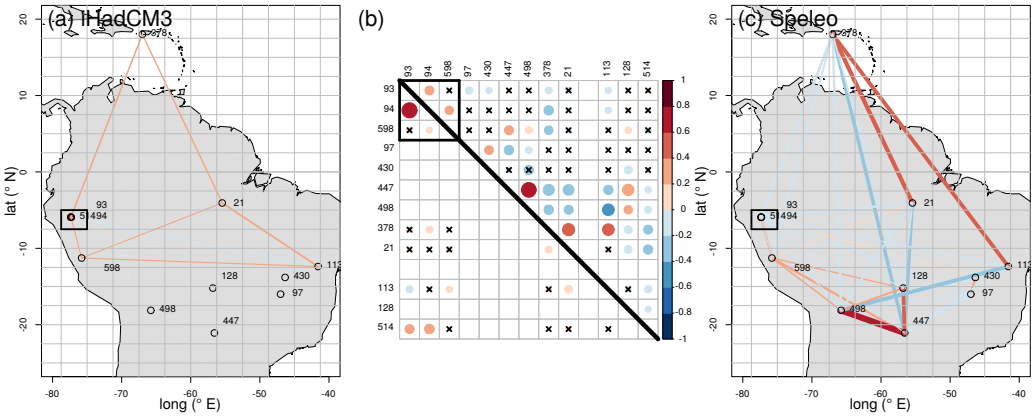

Figure S9. Network map and matrix comparison for the South America cluster (c2) as in SF7.

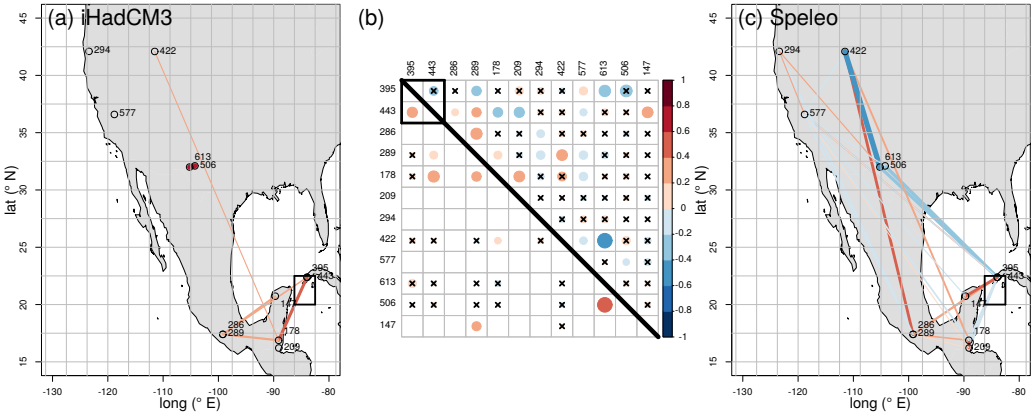

Figure S10. Network map and matrix comparison for the North America cluster (c3) as in SF7.

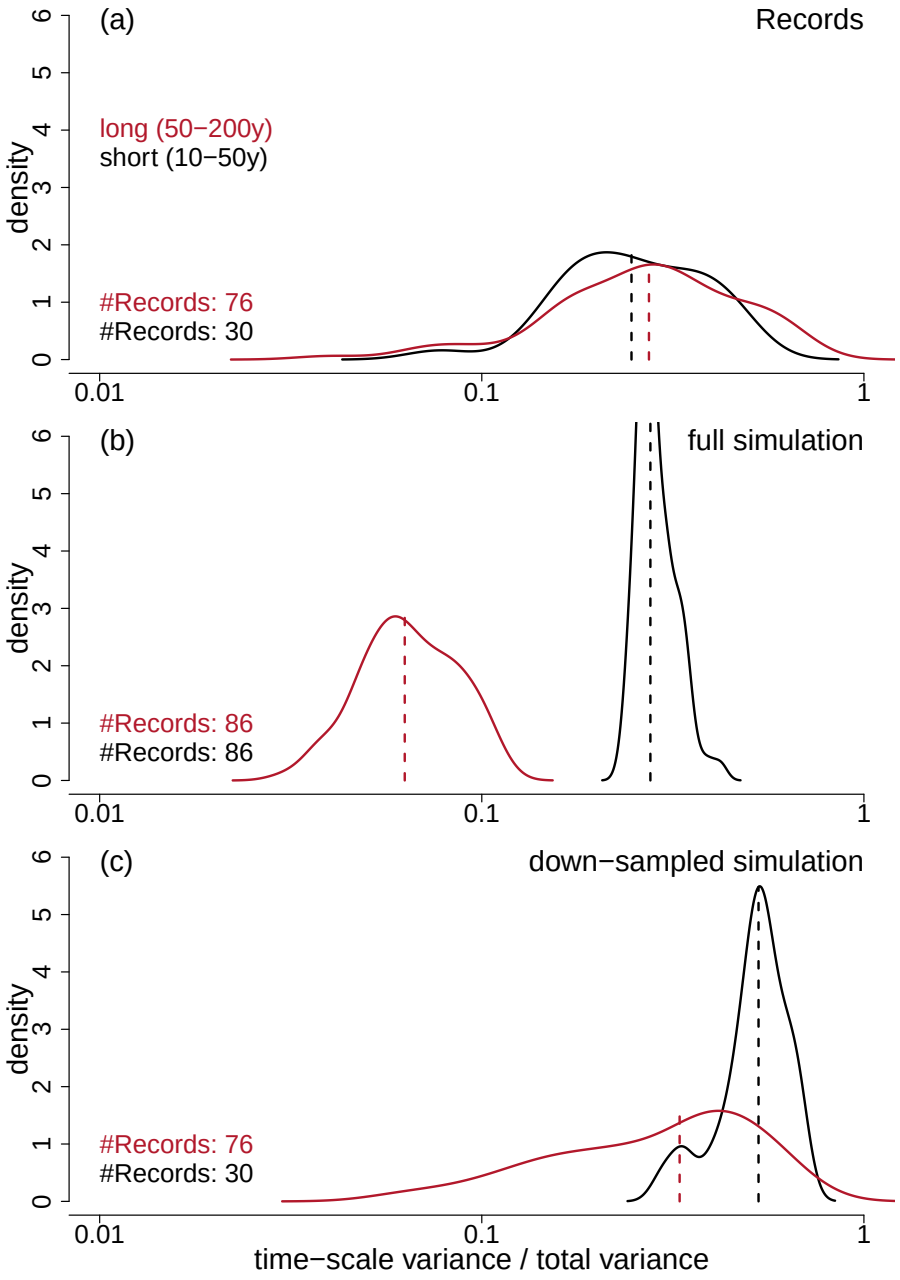

Figure S11. Variance on different time scales: density plots of the ratio of the time period variance to the total variance for (a) the record $\delta^{18}\mathrm{O}_{\mathrm{dw.eq}}$, (b) the simulation $\delta^{18}\mathrm{O}_{pw}$ with yearly resolution and (c) the simulated $\delta^{18}\mathrm{O}_{pw}$ down-sampled to record resolution. We look at the ratio between the variance on a longer timescale of 50-200y to the total variance (red) and on shorter time scales of 10-50y (black), and show the number of records for which the variance could be extracted respectively. The dotted lines show the medians of the distribution.

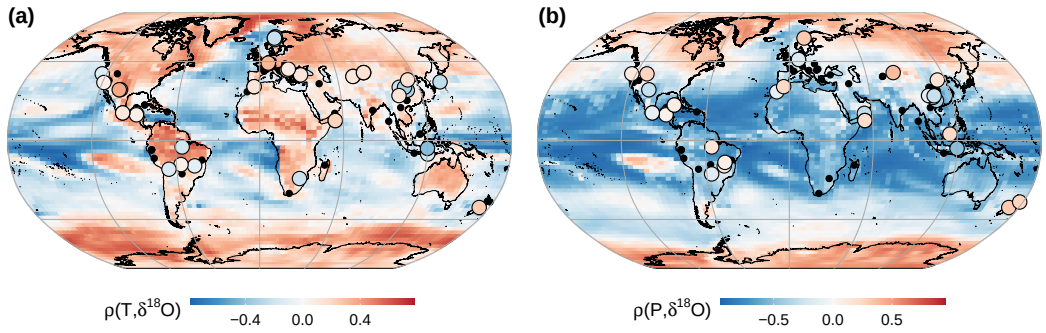

Figure S12. Seasonal correlation: Correlation plot for temperature (a) and precipitation (b) to $\delta^{18}O_{speleo}$ corresponding to Fig. 7. For each entity, we show the correlation estimate that was obtaines from tuning for the strongest absolut correlation to seasonal climate variables from S14. A blue point indicates, that the correlation estimate between $\delta^{18}O_{speleo}$ and the simulated seasonal climate variable on record resolution is significant and strongest during a season with negative correlation.

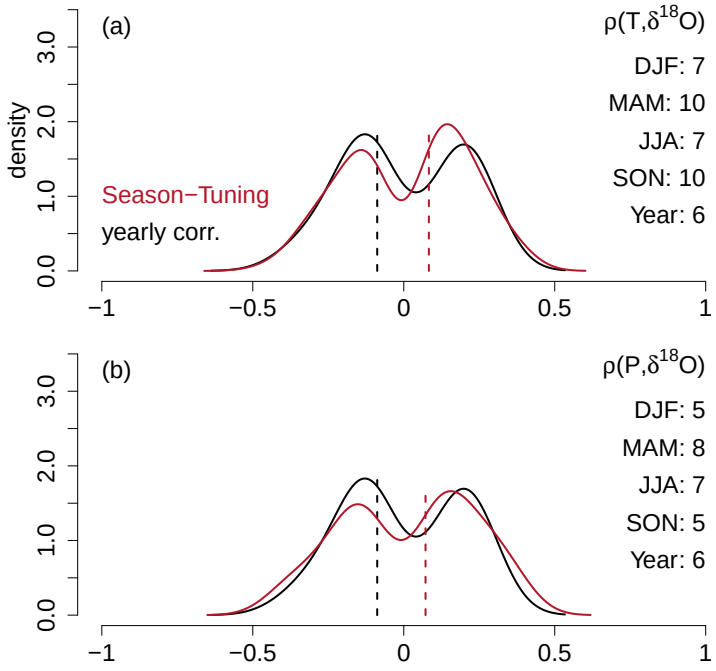

Figure S13. Seasonal correlation optimization: Density plot showing the correlation between simulated climate parameters at cave sites, temperature (a) and precipitation (b), and $\delta^{18}O_{speleo}$. The distribution shows the correlation to the yearly signal (black) and after tuning to the seasonal signal with the absolute strongest correlation (red) as in S14 and S12. All simulation ensemble members are used to plot the densities. The numbers on the side indicate the number of significant correlations per season for *xnapa*.

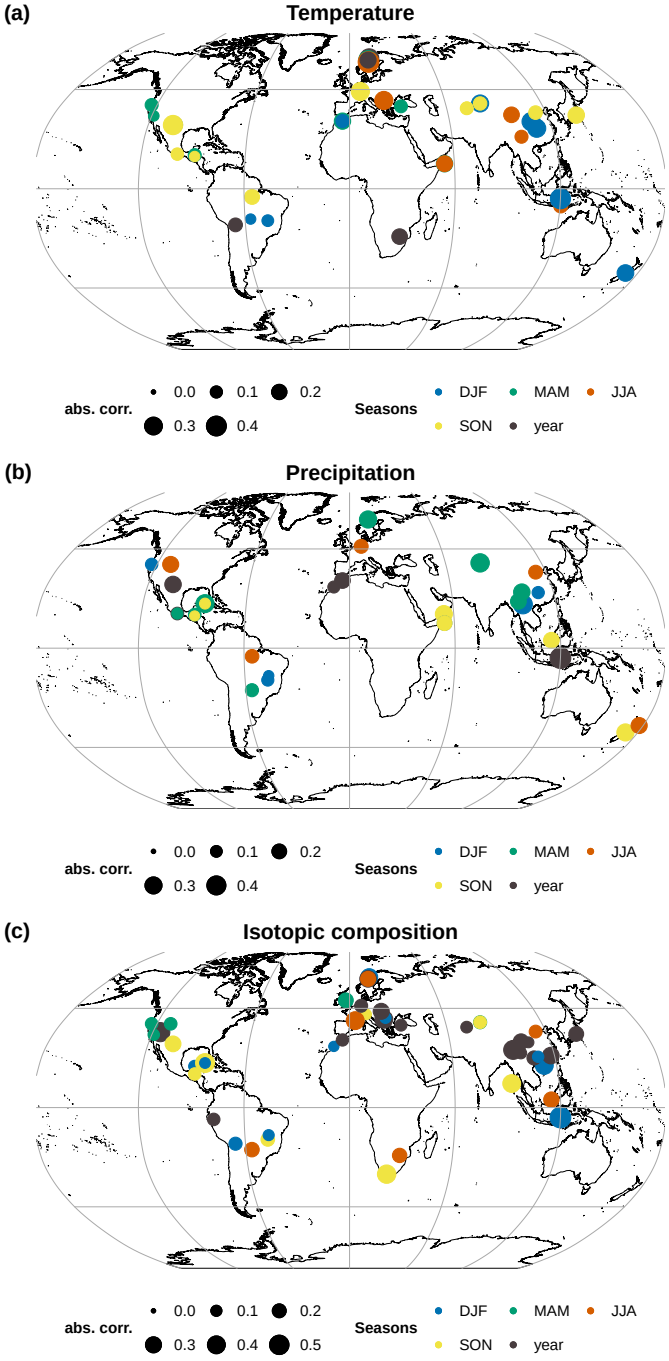

Figure S14. Seasonal signal: Correlation between the modeled seasonal climate signal over the last millennium ((a) temperature, (b) precipitaion amount, (c) mean seasonal $\delta^{18}O$ or yearly $\delta^{18}O_{pw}$) to $\delta^{18}O_{speleo}$. The dots show the abolute strength of the strongest seasonal correlation in size, and the season of strongest correlation in color (DJF, MAM, JJA, SON). Black dots indicate where the correlation at the annual scale is strongest.

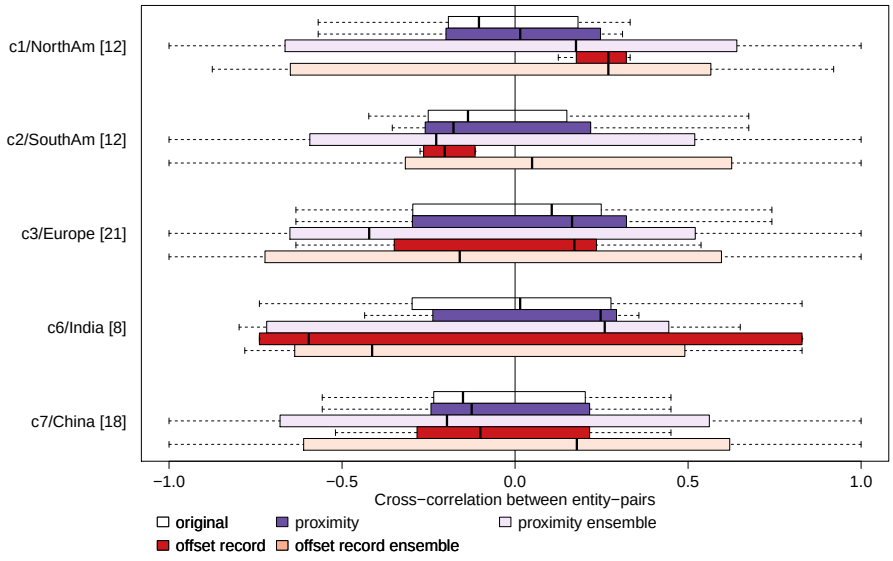

Figure S15. Network sensitivity to age-model selection: Comparing the sensitivity of spatial correlations (original, white) to spatial proximity and mean value offsets. For the proximity test (purple bars) only the 50% spatially closest locations were considered. For testing the effect of the offsets, only the 50% of the correlation matrix with a below-average mean offset wer considered. Seeking the strognest possible absolute correlation to the entire network, positive and negative values are amplified.

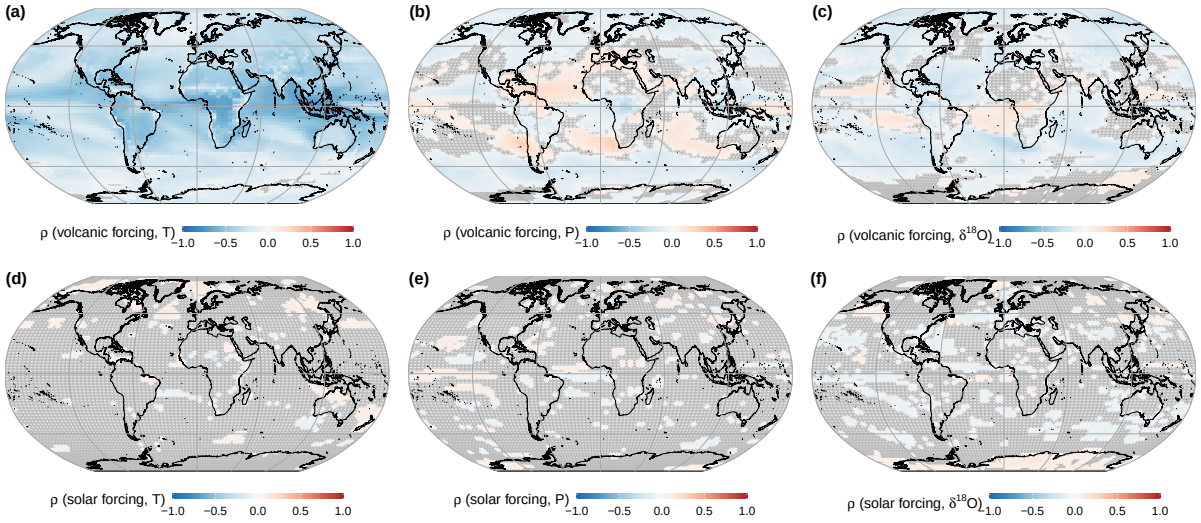

Figure S16. Correlation of solar and volcanic forcing with simulated climate variables: correlation estimate fields of a) ensemble mean simulated temperature, b) precipitation, and c) δ^{18}O to volcanic forcing, and the same ensemble mean climate variables to solar forcing d-f). Empty tiles mask gridboxes with $p > 0.1$. The area-weighted average correlation estimates with volcanic forcing are ρ(T,volc) = -0.34 (-0.48, -0.11), ρ(P,volc) = -0.04 (-0.15, 0.05), $\rho(\delta^{18}\mathrm{O}$,volc) = -0.08 (-0.18, 0.00). The area-weighted average correlation estimates with solar forcing are ρ(T,sol) = 0.01 (-0.004, 0.03), ρ(P,sol) = 0.003 (-0.009, 0.024), $\rho(\delta^{18}\mathrm{O}$,sol) = -0.012 (-0.035, 0.056). The correlation estimates per gridbox are calculated using the annual means over the time period of the last millennium (1000 yr) with 989 degrees of freedom.

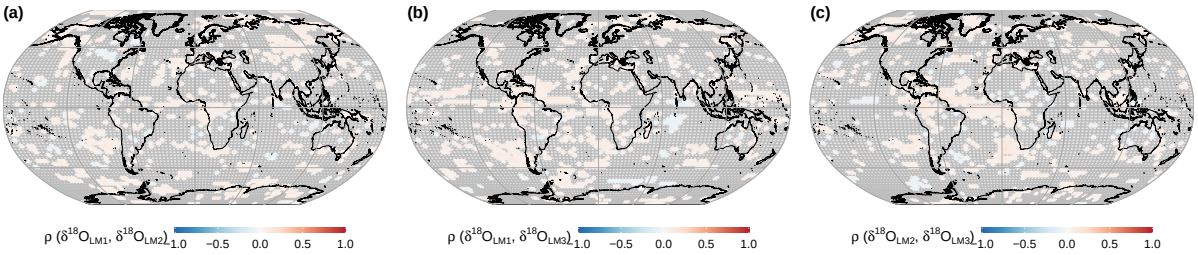

Figure S17. Independence of the initial condition ensemble members: correlation estimate fields of the simulated δ^{18}O of a) LM1 and LM2, b) LM1 and LM3, and c) LM2 and LM3. Empty tiles mask gridboxes with $p > 0.1$. The correlation estimates are calculated with 989 degrees of freedom.

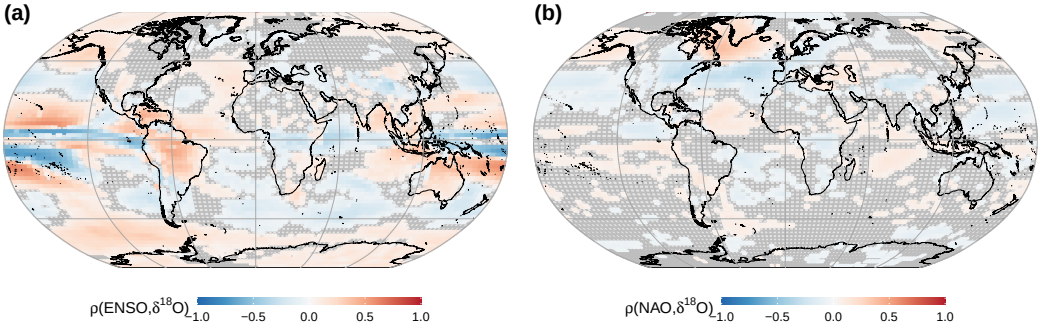

Figure S18. Isotope comparison to climatic modes: correlation estimate fields of the simulated δ^{18}O of LM1 to indices calculated from the simulation: a) ENSO as the Niño3.4 index, which is the equatorial 5°N-5°S area-averaged DJF mean temperature anomaly over the region 120-170°W (**?**), b) NAO index based on the first principal component of the DJF area-weighted sea level pressure anomaly between -90-40°W and 20-80°N (**?**). Empty tiles mask gridboxes with $p > 0.1$. The correlation estimates are calculated with 989 degrees of freedom.